TRENDS IN SCIENCES 2025; 22(10): 10615
https://doi.org/10.48048/tis.2025.10615 RESEARCH ARTICLE

Exploring Antibacterial Potential of Anhuienoside E from *Nigella sativa* Linn: A Promising Candidate Against Dental Caries *In Vitro* and *In Silico* Studies

Rizal Padilah[1], Dikdik Kurnia[1,*], Tri Mayanti[1] and Denny Nurdin[2]

[1]*Department of Chemistry, Faculty of Mathematics and Natural Sciences, Universitas Padjadjaran, West Java 45363, Indonesia*
[2]*Department of Conservative Dentistry, Faculty of Dentistry, Universitas Padjadjaran, Jawa Barat 40132, Indonesia*

([*]Corresponding author's e-mail: dikdik.kurnia@unpad.ac.id)

Received: 9 May 2025, Revised: 4 June 2025, Accepted: 15 June 2025, Published: 15 July 2025

Abstract

Dental caries is a chronic disease suffered by almost the entire population in the world. The main bacterium that causes dental caries is *Streptococcus mutans*, which has the enzyme glucosyltransferase as a virulence factor. Other fatogenic bacteria that play a role in exacerbating the biofilm form of dental caries such as *Streptococccus sanguinis* and *Enterococcus faecalis* have cell wall defenses catalyzed by the MurA enzyme. Chlorhexidine has been reported as a treatment for dental caries but has developed resistance over time. *Nigella sativa* L. seeds have been widely recognized to have many health benefits such as antibacterial, antioxidant and antifungal. The caries-causing antibacterial activity of *N. sativa* seeds has not been widely reported. The aim of this study was to isolate antibacterial compounds from *N. sativa* against *S. mutans, S. sanguinis, E. faecalis*, predict the mechanism of compounds and their derivatives by *in silico* molecular docking and pharmacokinetic analysis by ADMET and drug-likeness methods. Isolation of compounds was carried out by column chromatography with bioassay guidance, inhibitory mechanism and sugar substituent effects were predicted by *in silico* molecular docking, pharmacokinetics and drug-likeness analysis were predicted by ADMET and Lipinski rules. Anhuienoside E was successfully isolated from *N. sativa* extract and demonstrated antibacterial activity, which had moderate MIC and MBC values of 625 and 1000 µg/mL against *S. mutans, S. sanguinis, E. faecalis*. Anhuienoside E had moderate binding affinity value compared to its derivatives with ΔG values of −6.84 and −8.67 Kcal/mol against MurA and Gtf. ADMET pharmacokinetic analysis and drug-likeness evaluation suggest that Anhuienoside E and its derivatives may serve as non-toxic, non-oral drug candidates. In conclusion, Anhuienoside E has potential antibacterial activity to be developed as an alternative to chlorhexidine. The amount and type of sugar substituents greatly affect the antibacterial activity of Anhuienoside E.

Keywords: *Nigella sativa* L., Dental caries, Antibacterial, Anhuienoside E

Introduction

Dental caries is a chronic disease that affects nearly the entire global population. According to Indonesia's 2018 Basic Health Research (Riskesdas) data, 95% of children aged 5 to 6 years suffer from dental caries [1]. The main bacteria that causes dental caries is *Streptococcus mutans*. *S. mutans* secretes extracellular polysaccharides by glucosyltransferase enzymes and gives the signals to other bacteria to form colonies on the biofilm layer [2,3]. *Streptococcus sanguinis* and *Enterococcus faecalis* receiving signals from *S. mutans* work together to make a stronger biofilm layer into caries [4,5]. Both of these bacteria have cell walls composed of peptidoglycans, which are synthesized by the MurA enzyme. Various treatments of dental caries have been reported in previous studies. Chlorhexidine is one of antiseptics that has been used commercially. Chlorhexidine targets the destruction of bacterial cell membranes. The ability of bacteria to regulate the DltA operon causes the increasing of hydrophobicity on the surface of cell membranes so

chlorhexidine is becoming resistance [6]. Treatment of dental caries with more specific targets needs to be explored, one of which is by targeting the glucosyltransferase (Gtf) and Muramidase A (MurA) enzymes.

Gtf is an enzyme that catalyzes the synthesis of extracellular polysaccharides on the tooth surface. It is secreted by *Streptococcus mutans* as a virulence factor and breaks the glycosidic bond in sucrose, producing glucose and fructose. Glucose monomers are polymerized and act as a signal for other bacteria to form colonies on the teeth surface (biofilm) which then form caries [7].

MurA is the first enzyme that catalysed the formation of peptidoglycans to build bacterial cell wall. Uridine diphosphate N-acetylglucosamine is converted into UDP-MurNac by MurA enzyme. In the next stage, it will be attached to sugar molecules to form peptidoglycans. Therefore, inhibition of this enzyme becomes very potent so bacteria will grow abnormalities or die [8,9]. Exploration of natural compounds that have potential as caries antibacterials by *in silico* molecular docking of inhibitory mechanisms against MurA and Gtf enzymes needs to be done. One of the natural sources which has antibacterial agent is the seeds of Black Cumin (*Nigella sativa* Linn.).

N. sativa Linn. is an herbal plant and has been known for a long time among people in all parts of the world. The high benefits of this plant, especially in the seeds, make it often used as an alternative to conventional medicine. *N. sativa* seeds are widely used as an herbal medicine in Indonesia called “Jamu”. The method of use is pounded then boiled and filtered water. The efficacy of this “Jamu” is believed to treat various diseases such as inflammation, diabetes and cold medicine. Several researchers revealed the benefits of extracts from *N. sativa* seeds as antibacterial, antioxidant, immunomodulatory and antiviral [10,11].

The content of secondary metabolite compounds found in *N. sativa* seeds such as flavonoids, triterpenoids, saponins, alkaloids and essential oils provide diverse bioactivities [12]. Natural product compounds have diverse functional groups such as hydroxy, carbonyl, amine and ester. The role of these functional groups involves redox reactions in prokaryotic cells. So that the presence of functional groups from compounds in *N. sativa* will increase antibacterial activity [13-16]. The main compound isolated from the essential oil of *N.sativa* seeds is thymoquinone, which has potential therapeutic effects against atherosclerosis, cancer, and diabetes [17-19].

The treatment of dental caries with *N. sativa* seed compounds has not been widely reported. The study of the mechanism of inhibition of Gtf and MurA enzymes by compounds from *N. sativa* through molecular docking approach is very useful to know the treatment action of compounds. Therefore, compounds from *N. sativa* have the potential to be explored as natural caries drug candidates with a review of mechanism of action studies. This study aimed to identify antibacterial compounds from *N. sativa* seed extract effective against *S. mutans*, *S. sanguinis*, and *E. faecalis*. to determine their mechanisms of action targeting MurA and Gtf enzymes, and to predict their pharmacokinetic properties through ADMET and drug-likeness analyse.

Materials and methods

Isolation of anhuienoside E (1)

N. sativa seeds were obtained from Indonesian local market at Jl. Pasar Barat No.44, Kebun Jeruk, Andir, Bandung in July 2023. Dried *N. sativa* seeds were ground then macerated, extracted and purified using *n*-hexane, ethyl acetate, methanol and water solvents from Sigma Aldrich Co. Ltd. (St. Louis, MO, USA) and Merck Co. Ltd. A total of 2 kg of dried *N. sativa* seeds were ground and macerated using 4 liters of methanol for 3 days, then filtered and concentrated using a rotatory evaporator. The methanol extract was tested for antibacterial activity against *S. mutans* ATCC 25175, *S. sanguinis* ATCC 10556 and *E. faecalis* ATCC 29212 at concentrations of 1% - 5%. The extract that was known to have oral antibacterial activity was partitioned as much as 30 g using a normal phase chromatography column Silica G 60 F_{254} as much as 300 g. The extract was eluted by *n*-hexane, ethyl acetate, methanol and water of 300 mL for 3 times, respectively until get 11 fractions. The fraction that had good antibacterial activity with the large amount of mass was fraction 7 (F-7) (methanol fraction, 14.52 g) which is continued to the purification stage. Analysis of spot patterns in F-7 used TLC (Thin Layer Chromatography) ODS (Octadecylsilane) RP-18 F_{254S} and Silica G 60 F_{254} (Merck, Darmstadt, Germany). It was observed under UV light at wavelengths of 254 and 365 nm and sprayed

with 10% H_2SO_4 solution in ethanol (v/v). 1 g of F-7 was performed column chromatography using ODS RP-18 F_{254S} and elution was performed using 30 mL of a methanol–water mixture (9:1, v/v) with a 2 %v/v gradient of increasing polarity, resulting in 32 subfractions. Huang [20] Column results were analyzed using TLC and observed the stain pattern under UV light 254 and 365 nm, then sprayed with H_2SO_4 10% stain reagent in ethanol (v/v) [21].

Structure elucidation of compound 1

Structure elucidation of Compound 1 was conducted by spectroscopic instruments. Identification of functional groups of compound 1 using Infrared spectrophotometer (FTIR Shimadzu 8400) Evangelina *et al.* [22], identification of proton and carbon chemical environment of compounds with 1D and 2D spectra (^{1}H-NMR, ^{13}C-NMR, DEPT 135°, HMQC, ^{1}H-^{1}H COSY, HMBC) using BRUKER NMR spectrometer AVANCE NEO 700 MHz series. Molecular mass measurement of compounds using Mass Spectrometer (MS Aquity TQD, Waters Corporation, MA, USA) [23].

Antibacterial testing

The methanol extract of *N. sativa* seeds was tested for antibacterial activity against *S. mutans* ATCC 25175, *S. sanguinis* ATCC 10556 and *E. faecalis* ATCC 29212 at concentrations of 1% - 5% by disc diffusion method. Positive control (chlorhexidine 2%), negative control methanol and extract as much as 20 µL were placed on paper disks and then placed on Muller Hinton agar media (purchased from Merck Co. Ltd. and Sigma Aldrich) containing 100 µL bacteria ½ McFarland. Agar media was incubated for 24 h at 37 ℃. Determination of the active fraction used the same procedure as the *N. sativa* seed methanol extract assay.

MIC testing was carried out on compound 1 by microdilution method at a concentration of 2% using microplate-96 wells. All wells of microplate-96 wells were filled with Muller Hinton liquid media, then 100 µL of methanol solvent was added as control. Compound 1 was added to the wells without methanol as much as 100 µL. Dilutions were performed by the microdilution method on Microplate-96 wells. Bacteria with a turbidity level of 0.5 McFarland as much as 5 µL were added to the wells. The microplate-96 wells were incubated for 24 h at 37 °C. After incubation, the absorbance was observed on the Biochrom EZ Read 400 ELISA tool with a wavelength of 620 nm and the MIC value was obtained. MBC testing is done by spreading clear media microplate-96 wells containing compound 1 and bacteria on Muller Hinton agar media then incubated at 37 °C for 24 h so that the MBC value can be determined [24]. Antibacterial testing of zone of inhibition was performed in triplicate, MIC and MBC were performed in duplicate.

***In silico* molecular docking**

Preparation of docking

The enzymes used in molecular docking were MurA and Gtfs which have PDB ID: 8FKL Schormann *et al.* [25] and 1UAE Kurnia *et al.* [26] whose 3D structures were downloaded on the website www.rcsb.org. Conformation validation of MurA and Gtf enzymes using Ramachandran Plot [27]. The 2 Ramachandran-conforming enzyme PDB codes 8FKL and 1UAE were separated with bile and ligand natives using the Biovia discovery studio. Coordinates of the enzyme active site were analyzed on the web server http://sts.bioe.uic.edu/castp/index [28]. Enzyme preparation using Biovia Discovery Studio 2021 software. The structures of compound 1 and its derivatives were drawn in ChemDraw 15.0 and energy minimization was performed in Chem3D Ultra 8.0. Chlorohexidine and apigenin as positive controls were downloaded on the page https://pubchem.ncbi.nlm.nih.gov with CID: 9552079 and 5280443 codes.

Molecular docking

Molecular docking was run using AutoDockTools-1.5.7 software [29]. Receptors (Gtf and MurA) were pretreated by adding Kollman charge while ligands compound 1, derivates and positive control were added to Compute Gasteiger. Docking was performed on receptor active site regions obtained from calculations on the CASTp webserver. Docking parameters using Genetic algorithms with 100 runs. Visualization of docking results (type of interaction and number of interactions) was observed in Biovia discovery studio. Adding grid box area is better

ADMET and drug-likeness analysis

ADMET analysis of compound 1 and derivatives using web server https://biosig.lab.uq.edu.au/pkcsm. The chemical structure of compound 1 and its derivatives is made in smile format which is drawn on the web http://www.swissadme.ch. Determination of drug-likeness using web server https://tox.charite.de/protox3 [30-32].

Results and discussion

Isolation of compounds from *N. sativa* seeds

Maceration of 2 kg of *N. sativa* seeds using 4L methanol was concentrated to obtain 46.5 g of extract. The methanol extract of *N. sativa* seeds was tested for antibacterial activity against *S. mutans, S. sanguinis* and *E. faecalis* through inhibition zone test. The test results of the extract showed active as antibacterial against the 3 bacteria (test results are in **Table 1**) which indicated the compound components potentially as antibacterial agent [33]. The methanol extract was further fractionated into 11 fractions and tested for antibacterial activity. Based on the results of antibacterial testing of the 11 fractions, it showed that fraction 7 had good oral antibacterial activity, so it was continued to the purification stage (test results are in **Table 2**). The isolation of compounds from the active fraction aims to obtain the most active isolate. Some isolates showed more active antibacterial activity than the fraction and others were less active depending on their nature in the antagonistic or synergistic fraction [34].

Fraction F-7 from the initial partition was purified using ODS RP-18 $F_{254}S$ chromatography column with 2% gradient H_2O-methanol eluent starting from 9:1 solvent ratio until 32 fractions were obtained. The purification results were analyzed using TLC. Based on the KLT analysis on the ODS RP-18 plate, F-7-30 (100 mg) has a single stain that does not fluoresce under UV lights 254 and 365 nm and is brown after being sprayed with H_2SO_4. This fraction is thought to be a pure isolate which is called compound 1 [35,36].

Table 1 The results of the inhibition test of *N. sativa* seed methanol extract against 3 oral pathogenic bacteria

No	Bacteria	1%	2%	3%	4%	5%	Chlorhexidine (2%)
		M ± SD	M ± SD	M ± SD	M ± SD	M ± SD	M ± SD
1	*S. mutans* ATCC 25175	nd	nd	nd	6.9 ± 0.15	10.5 ± 0.1	17.8 ± 0.1
2	*S. sanguinis* ATCC 10556	nd	nd	nd	8.7 ± 0.05	8.9 ± 0.05	21.9 ± 0.05
3	*E. faecalis* ATCC 29212	11.2 ± 0.1	12.2 ± 0.05	13.2 ± 0.05	14.5 ± 0.05	15.9 ± 0.05	17.3 ± 0.05

Abbreviation: nd (Note Determine), mm (millimeters), M (mean), SD (Standard Deviation)

Table 2 Inhibition zone test results of fractions 1-11 of *N. sativa* seed methanol extract against 3 oral pathogenic bacteria.

No	Bacteria	Inhibition Zone (mm) at 5% Concentration											
		1 M ± SD	2 M ± SD	3 M ± SD	4 M ± SD	5 M ± SD	6 M ± SD	7 M ± SD	8 M ± SD	9 M ± SD	10 M ± SD	11 M ± SD	Chlorhexidine (2%) M ± SD
1	*S. mutans* ATCC 25175	nd	7.5 ± 0.1	8.9 ± 0.1	8.3 ± 0.05	7.3 ± 0.1	7.7 ± 0.1	7.2 ± 0.1	-	-	-	-	17.8 ± 0.0
2	*S. sanguinis* ATCC 10556	nd	9.5 ± 0.1	9.0 ± 0.15	9.0 ± 0.1	8.9 ± 0.05	9.6 ± 0.1	9.7 ± 0.1	8.6 ± 0.15	8.4 ± 0.05	8.7 ± 0.1	8.8 ± 0.15	21.9 ± 0.0
3	*E. faecalis* ATCC 29212	nd	nd	13.4 ±	14.4 ± 0.1	nd	nd	8.6 ± 0.1	nd	nd	nd	10.9 ± 0.15	17.25 ± 0.0

Abbreviation: nd (Note Determine), mm (millimeters), - (no inhibition), M (mean), SD (Standard Deviation)

Structure elucidation of compound (1)

The results of measurements using IR spectrophotometer indicated that compound 1 has an OH group at υ_{maks} 3367 cm^{-1}, C-H sp^3 stretch at υ_{maks} 2940 cm^{-1}, C=O stretch vibrations at υ_{maks} 1634 cm^{-1}, aliphatic C=C stretch vibrations at υ_{maks} 1455 cm^{-1}, gem dimethyl $C(CH_3)_2$ stretch vibrations at υ_{maks} 1385 cm^{-1}, C-O stretch vibrations at υ_{maks} 1058 cm^{-1}, and alkene C-H bending at υ_{maks} 635 cm^{-1} [37].

Chemical shift of carbon compound (1) (brown solids, 100 mg) showed ^{13}C-NMR (CD_3OD, 700 MHz) δ 13.8 ppm (C-1), 16.6 ppm (C-2), 17.8 ppm (C-3), 17,9 ppm (C-4), 18.0 ppm (C-5), 18.8 ppm (C-6), 23.9 ppm (C-7), 24.2 ppm (C-8), 24.6 ppm (C-9), 26,4 ppm (C-10), 26.6 ppm (C-11), 28.9 ppm (C-12), 31.6 ppm (C-13), 33.3 ppm (C-14), 33.3 ppm (C-15), 33.5 ppm (C-16), 34.8 ppm (C-17), 37.6 ppm (C-18), 39.7 ppm (C-19), 40.6 ppm (C-20), 42.5 ppm (C-21), 43.9 ppm (C-22), 44.0 ppm (C-23), 47.1 ppm (C-24), 48.0 ppm (C-25), 48.1 ppm (C-26), 49.9 ppm (C-27 Rha), 61.8-82.4 ppm (C-(28-52 sugar), 95.7, 101.3, 104.2, 104.6 and 106.5 ppm (C-(53-57anomeric), 123.7 ppm (C-58), 144.0 ppm (C-59), 178.0 ppm (C-60); ^{1}H-NMR (CD_3OD, 700 MHz) δ 0.72 ppm (3H, s; H-1), 0.82 ppm (3H, s; H-4), 0.94 ppm (3H, s; H-16), 0.97 ppm (3H, s; H-8), 1.00 ppm (3H, s; H-2), 1.19 ppm (3H, s; H-10), 1.25 ppm (2H, t J = 6, H-14), 1.28 ppm (3H, s; H-3), 1.29 ppm (3H, s; H-5), 1.39 ppm (2H, t; J = 12, H-17), 1.51 ppm (2H, t; J = 12, H-6), 1.63 ppm (2H, t; J = 6, H-7), 1.64 ppm (3H, s; H-28), 1.67 ppm (4H, t; J = 6, H-9&15), 1.71 ppm (4H, t; J = 6, H-11&12), 1.78 ppm (2H, d; J = 6, H-24), 1.79 ppm (2H, q; J = 6, H-24), 1.92 ppm (1H, t; J = 6, H-27), 1.93 ppm (1H, t; J = 6, H-25), 2.89 ppm (1H, q; J = 6, H-21), 3.87 ppm (1H, t; J= 6; H-52), 3.89 ppm (1H, t; J= 6; H-58), 3.90-4.1 ppm (21H; H-sugar), 4.42 ppm (1H, d; J= 7.8 H-55 anomeric), 4.51 ppm (1H, d; J = 7,5 H-57 anomeric), 4.55 ppm (1H, d; J = 6.2 H-56 anomeric), 5.26 ppm (1H, d; J = 16.3 H-54 anomeric), 5.36 ppm (1H, d; J = 8.1 H-53 anomeric). ^{1}H, ^{13}C- and 2D-NMR chemical shift data of compound 1 are shown in **Tables 3** and **4**.

Based on the ^{13}C-NMR data, compound 1 contained 60 types of carbon. DEPT, ^{1}H-NMR spectrum and HSQC correlation showed compound 1 contained 8 quaternary carbons, 5 methine carbons, 24 oxidized methine carbons, one sp^2 methine, 9 methyl, and thirteen methylene. HMBC spectrum shows proton to-carbon correlation as far as 2 to 5 bonds and the COSY spectrum shows proton to proton correlation as far as 3 bonds are suspected of compound 1 being a burnt triterpenoid group [38]. Carbon 60 and carbon 52 experienced the addition of sugar substituents as many as 5 pieces shown by the presence of carbon and anomeric protons as many as 5. Three sugars namely glucose'- glucose"-rhamnose' were bound to carbon 60 and 2 glc-rha sugars at carbon 52. The placement of the number and type of sugar was based on the HMBC correlation of the anomeric proton to carbon 60 and 52 proton to anomeric carbon. Shi *et al.* [39] Configuration of sugar group in compound 1 was β which was indicated by the shear of the anomeric carbon ≥ 99 and α at ≤ 95 [40,41]. NMR spectrum showed that compound 1 had the molecular formula $C_{60}H_{98}O_6$ with a degree of unsaturation of 12. Measurement of the molecular mass of compound 1 using a Water Acquit UPLC type triquadrupole $[M+Na]^+$ at *m/z* 1257 confirmed the alleged structure of compound 1 (Shown in **Figure 1**) [42]. Based on the literature, compound 1 has proton and carbon chemical shifts similar to Anhuienoside E isolated from *N. sativa* seeds. In addition, based on MS measurements, it has a similar molecular weight, thus confirming that compound 1 is Anhuienoside E (all spectra in **Figures S(1) - S(7)**) [43].

Table 3 Chemical shift data of ^{1}H, ^{13}C- and 2D-NMR of compound **1**.

No.C	δc (ppm)	δH (ppm) (ΣH; multiplicity; *J* (Hz))	HMBC		COSY
			^2J	^3J	
1	13.8	0.72 (3H; *s*)	-	-	-
2	16.6	1.00 (3H; *s*)	-	-	-
3	17.8	0.82 (3H; *s*)	-	-	-

No.C	δc (ppm)	δH (ppm) (ΣH; multiplicity; *J* (Hz))	HMBC		COSY
			^{2}J	^{3}J	
4	17.9	1.29 (3H; *s*)	-	H-1	-
5	18.0	1.29 (3H; *s*)	-	-	-
6	18.8	1.29 (2H; *d*; 6)	-	-	-
7	23.9	1.67 (1H; *d*;6)	-	-	-
8	24.1	0.82 (3H; *s*)	-	-	-
9	24.5	1.78 (2H; *q*; 12*)*	-	-	-
10	26.4	0.94 (3H; *s*)	-	-	-
11	26.6	3.65 (2H; *d*; 12)	-	-	-
12	28.9	1.92 (2H; *t*; 12)	-	-	-
13	31.6	-	H-8, H-13	-	-
14	33.3	1.71 (2H; *t*; 12)	-	-	-
15	33.3	1.28 (1H; *d*; 12)	-	-	-
16	33.5	1.6 (1H; *d*; 12)	-	-	-
17	34.8	1.19 (3H; *s*)	-	-	-
18	37.6	-	H-2	-	-
19	39.7	3.27 (2H; *t*; 6)	-	-	-
20	40.57	-	H-3, H-5	-	-
21	42.47	3.35 (2H; *t*; 6)	-	-	-
22	43.9	-	-	-	-
23	43.9	-	-	-	-
24	47.2	3.27 (2H; *t*; 6)	-	-	H-25
25	48.0	1.63 (2H; *d*; 6)	-	H-2	H-24
26	48.1	-	-	-	-
27	48.2	2.89 (1H; *d*; 6)	-	H2	-
28	49.8	3.93 (1H; *d*; 6)	-	-	-
29	61.8	3.86 (2H; *d*; 6)	-	-	-
30	64.6	3.79 (2H; *d*; 6)	-	-	-
31	69.8	3.55 (2H; *d*; 6)	-	-	-
32	66.9	3.72 (1H; *s*)	-	-	-
33	70.6	3.42 (1H; *s*)	-	-	-
34	70.8	3.93 (1H; *d*; 6)	-	-	-
35	70.9	3.99 (1H; *d*; 6)	-	-	-
36	71.0	3.48 (1H; *d*; 6)	-	-	-
37	72.1	3.44 (1H; *d*; 6)	-	-	H-57
38	72.3	3.59 (1H; *d*; 12)	-	-	-
39	72.7	3.65 (1H; *d*; 6)	-	-	-
40	737	3.68 (1H; *d*; 6)	-	-	H-53

No.C	δc (ppm)	δH (ppm) (ΣH; multiplicity; *J* (Hz))	HMBC		COSY
			^{2}J	^{3}J	
41	73.7	3.09 (1H; *d*; 6)	-	-	-
42	74.1	4.10 (1H; *d*; 12)	-	-	-
43	75.2	3.59 (1H; *d*; 12)	-	-	-
44	76.1	3.59 (1H; *d*; 12)	-	-	-
45	76.6	3.59 (1H; *d*; 12)	-	-	-
46	76.7	3.59 (1H; *d*; 12)	-	-	-
47	77.5	3.53 (1H; *d*; 12)	-	-	-
48	77.9	3.68 (1H; *d*; 6)	-	-	-

Table 4 Chemical shift data of ^{1}H, ^{13}C- and 2D-NMR of compound 1.

No.C	δc (ppm)	δH (ppm) (ΣH; multiplicity; *J* (Hz))	HMBC		COSY
			^{2}J	^{3}J	
48	77.9	3.68 (1H; *d*; 6)	-	-	-
49	78.1	3.59 (1H; *d*; 12)	-	-	-
50	79.5	3.53 (1H; *d*; 12)	-	-	-
51	82.0	3.68 (1H; *d*; 6)	-	-	-
52	82.3	3.59 (1H; *d*; 12)	-	-	-
53	95.7	5.35 (1H; *d*; 6)	-	H-30	H-40
54	101.3	5.27 (1H; *d*; 12)	-	H-28	-
55	102.7	4.42 (1H; *d*; 6)	-	H-52	-
56	104.0	4.53 (1H; *d*; 12)	-	H-10	-
57	104.6	4.50 (1H; *d*; 6)	-	H-30, H-29	H-37
58	123.7	3.90 (1H; *m*; 6)	-	-	-
59	144.0	-	-	-	-
60	178.0	-	-	H-53	-

Antibacterial testing of anhuienoside E (1)

Antibacterial testing of Anhuienoside E (1) against *S. mutans, S. sanguinis* and *E. faecalis* was carried out by microdilution method. The test results are in **Table 5** which showed moderate activity with MIC values of 625 μg/mL and MBC of 1000 μg/mL [44]. Anhuienoside E (1) showed that did not give activity for killing *E. faecalis* but only gave inhibition activity. Anhuienoside E had 5 sugar groups and other functional groups such as alkenes and carbonyls that could inhibit bacteria through the destruction of cell membranes and inhibit enzymes that have important catalytic activities in bacteria [45]. The moderate MIC values were very relevant to MBC values that were in the inactive range. The study of the antibacterial mechanism of Anhuienoside E (1) and the effect of sugar groups on antibacterial activity was predicted by molecular docking against key pathogenic enzymes of oral bacteria.

Table 5 MIC and MBC test results of Anhuienoside E (1) against 3 oral pathogenic bacteria.

No.	Bacteria	MIC (μg/mL)	MBC(μg/mL)
		M ± SD	M
1	*S. mutans* ATCC 25175	625 ± 0.05	1000
2	*S. sanguinis* ATCC 10556	625 ± 0.05	1000
3	*E. faecalis* ATCC 29212	625 ± 0.1	-

Abbreviation: MIC (minimum inhibition concentration), MBC (minimum bactericidal concentration), - (inactive) M (mean), SD (Standard Deviation).

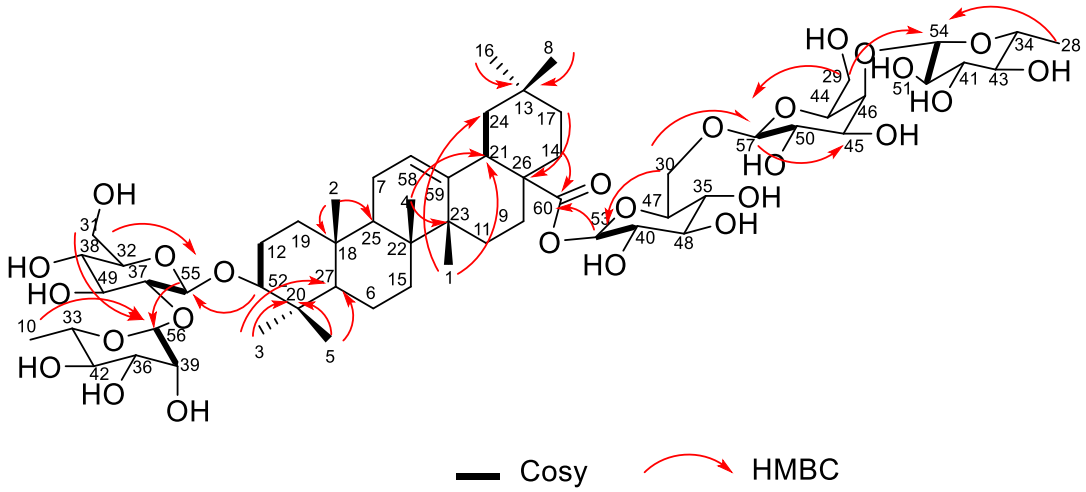

Figure 1 Structure of Anhuienoside E (1) with thick line COSY spectrum correlation and red line HMBC correlation.

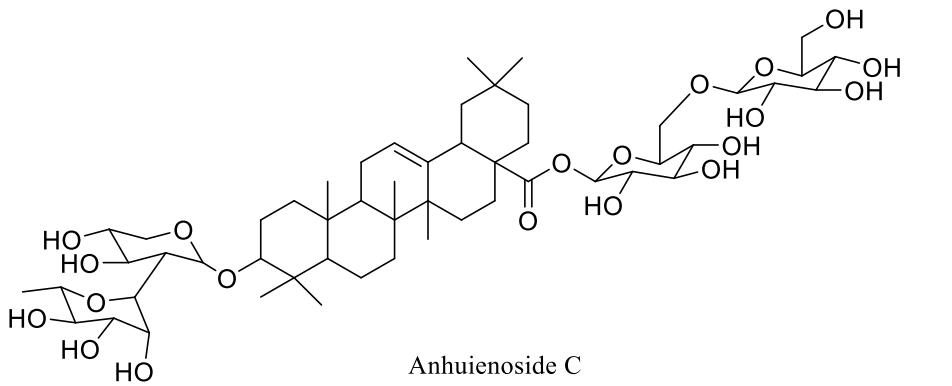

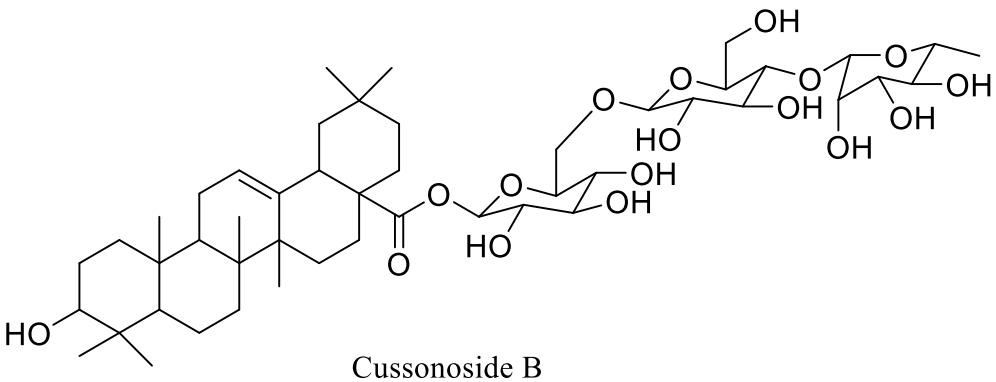

Figure 2 Chemical structure of Anhuienoside C (derivate 3) and Cussonoside B (derivate 5).

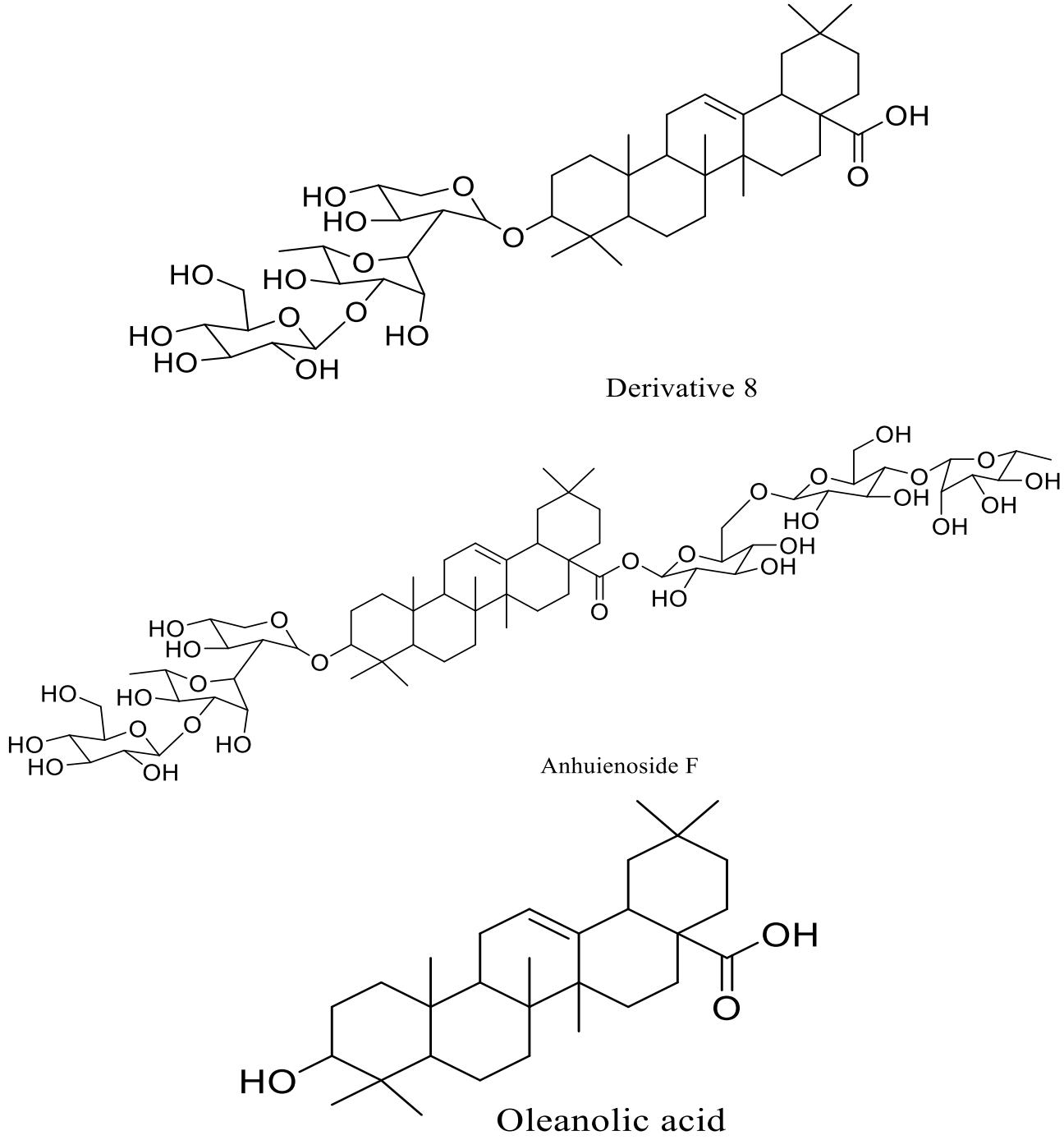

Figure 3 Chemical structure of Anhuienoside D (derivate 2), derivate 8, Anhuienoside F (derivate 4), and Oleanolic acid (derivate 9).

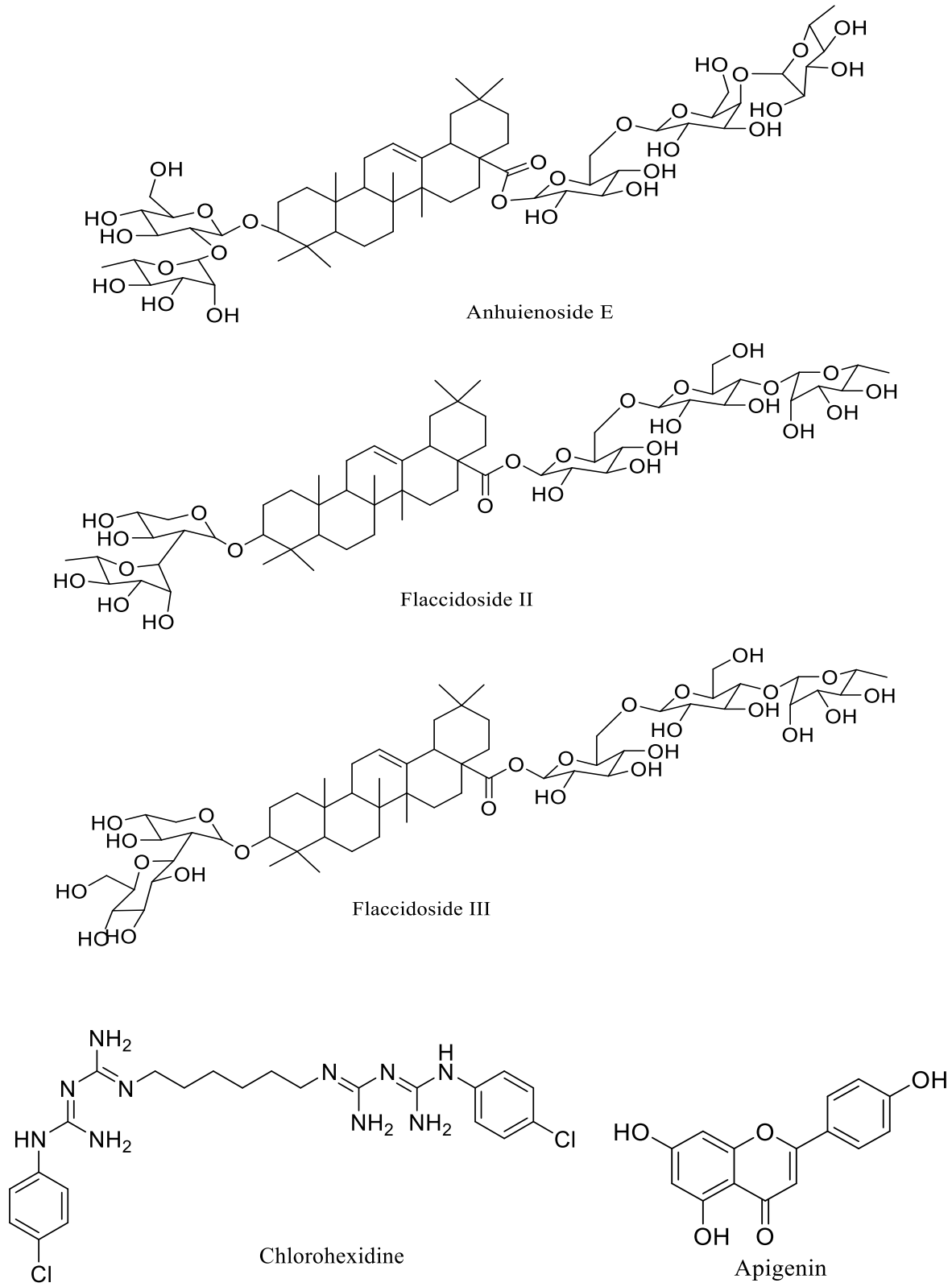

Figure 4 Chemical structure of Anhuienoside E (1), Flaccisdoside II (derivate 6), Flaccisdoside III (derivate 7), chlorhexidine and Apigenin (positive control).

Molecular docking

Molecular docking was performed on Anhuienoside E (1) and derivates on 2 key enzymes from caries-causing bacteria (the structures are shown in **Figures 2** - **4**). MurA enzyme was an enzyme that catalysed peptidoglycan at the initiation stage

representing *E. faecalis* and *S. sanguinis* bacteria. Gtf enzyme with PDBID 8FKL isolated from *S. mutans* catalysed the formation of extracellular polysaccharides starting from the cleavage of sucrose glycosides [46]. Both enzymes were analysed for conformational similarity of amino acid bile before characterization and after visualization in the protein data bank using the Ramachandran plot. Ramachandaran plot describes the conformation of α-helical and β-sheet bonds in protein peptides with 2 coordinate torsions ϕ and ψ (ψ 180, ϕ > 0). Based on the Karplus equation, the Ramachandran plot was divided into 4 regions to determine whether the conformation of amino acids was still stable during X-ray and does not damage the α-helical and β-sheet bonds. One [A, B, L] region was highly favoured, additional allowed regions [a, b, l, p], generously allowed regions [~a, ~b, ~l, ~p] and disallowed regions as shown in **Figure 5**. Amino acid residues from proteins that will be used for molecular docking should not occupy disallowed regions of more than 2% to ensure conformational conformity with the actual protein structure [47-49]. Both MurA and Gtf have a disallowed region value of 0%, indicating that their conformations are consistent with the original structures and can be used for *in silico* molecular docking.

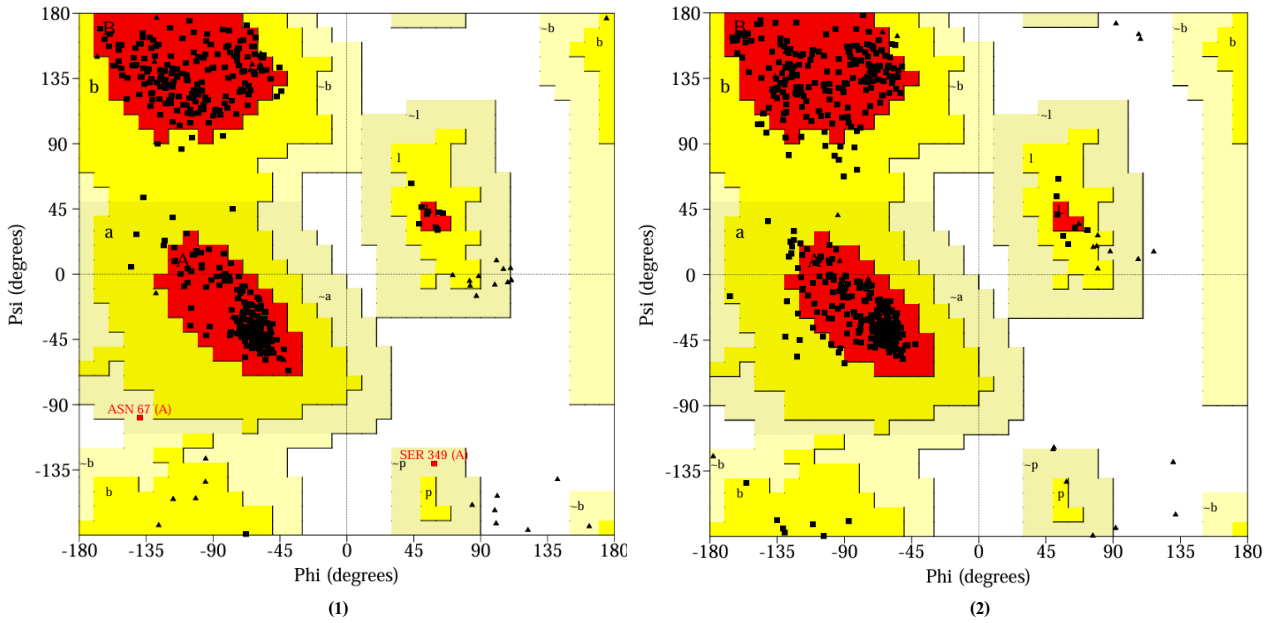

Figure 5 Ramachandran plot of MurA enzyme (1) and Gtf enzyme (2).

Anhuienoside E (1), Anhuienoside C (3), Anhuienoside D (2), Anhuienoside F (4), Cussonoside B (5), Flaccidoside II (6), and Flaccidoside III (7), Derivate (8), Oleanolic acid (9), chlorhexidine, apigenin were docked with MurA and Gtf enzymes. Compounds 1-9 were subjected to molecular docking to compare their inhibitory activity against MurA and Gtf enzymes, with a focus on variations in the number and type of sugar substituents. Sugar groups had many hydroxyl functional groups that can interact by hydrogen bond with enzymes. Molecular docking results demonstrate that sugar groups significantly influence the strength of interactions between ligands (compounds) and receptors (enzymes), as characterized by varying delta G (ΔG) values, as shown in **Figures 5** and **6**. ΔG is a parameter representing the strength of ligand-receptor binding, measured in kcal/mol, and is derived from the following equation:

$$\Delta G = -RT \ln K \quad (1)$$

The ΔG value decreases as the K value (the equilibrium constant between protein and ligand) increases [50]. The greater the value of K the reaction goes towards the product or the stronger the protein-ligand association. Docking is performed at the receptor (enzyme) active site, meaning the ligand (compound) acts as a competitive inhibitor against the native ligand

or cofactor. Ligand binding in the active site region can alter enzyme stability or inhibit its activity [51].

Anhuienoside E (1) had a relatively moderate ΔG value compared to other compounds and positive controls against the MurA enzyme. The number of glucose units significantly affects ligand–protein binding affinity, as evidenced by Anhuienoside F (4), which exhibited the lowest binding affinity (the highest ΔG value) toward MurA among the tested compounds, due to the presence of 6 sugar groups (**Figure 6**). The results of docking visualization in **Figure 8** showed that almost all compounds interact with ligands through sugar groups excepted compounds 4 and 7 with carbonyl esters. Sugar groups covered other functional groups in terpenoid structure because the interactions formed (hydrogen bonds) were stronger. MurA enzyme structure was also relatively small, so bulk compounds such as Anhuienoside E were difficult to interact with the active site area. MurA facilitates glycosidic bond formation in peptidoglycan biosynthesis, and the presence of sugar groups may disrupt this activity, preventing bacterial cell wall formation. The type of sugar affected the value of ΔG. Almost all compounds (1-8) interacted by hydrogen bond with the enzyme through the sugar rhamnose. The hydroxy position at number 4 on rhamnose tended to be the most electronegative because there was an EDG (electron donating group) group, namely either of C-anomeric and hydroxy group at carbon 5 which pushed electrons through the induction effect [52]. Compound 9 did not show the lowest ΔG value, likely due to the formation of a single hydrogen bond, highlighting the influence of the type and number of sugar groups on MurA enzyme inhibition. In addition, the positive control, chlorhexidine, did not show a higher ΔG value than some of the tested compounds (1-9), suggesting that Anhuienoside E, with proper derivatization, has potential as an alternative to chlorhexidine.

The docking results of compounds 1-9 with Gtf enzyme showed various ΔG values (shown in **Figure 7**). Flaccisdoside III (7) exhibited the lowest ΔG value through its interaction with the Gtf enzyme, specifically at the Glc'-Glc'' glycosidic bond (**Figure 9**). The Gtf enzyme catalyzes the synthesis of extracellular polysaccharides, initiating the process by cleaving the glycosidic bond of sucrose (Glc–fructose) [7]. The presence of Flaccisdoside III (7) in the active site region decreased the catalytic activity of the enzyme through hydrogen bonds formed from aspartic amino acids with Glc'-acid protons and Glc'-oxygen. In addition, in other compounds 1-8 there were hydrogen bonds (Shown in **Figure 9**) with Gtf which were very dominant from Glc to Gtf amino acid residues in the active site region. Anhuienoside E had inhibitory activity similar to the positive control Apigenin as shown by the ΔG values in **Figure 7**. This finding is supported by the number of hydrogen bond interactions formed by the glucose moieties of Anhuienoside E. All sugar-containing derivatives demonstrated stronger inhibitory activity against the Gtf enzyme compared to the positive control.

ADMET and drug-likeness analysis

ADMET analysis results of compounds 1-9 are show in **Table 6**. Analysis of Absorption (A), Distribution (D), Metabolism (M), Excretion (E) and Toxicity (T) was conducted to investigate the feasibility of these as antibacterial drugs. Absorption parameters (Intestinal Absorption and Water Solubility) indicated the drug's ability to be absorbed by the body based on its water solubility. The range of water solubility was log 95% of drugs: −6.0 to 0.5 [53]. Only compounds 5, 8 and 9 were absorbed by the body and the rest were carried by the blood to all body tissues. This data showed that Anhuienoside E, can reach the target of pathogenic bacteria. Distribution parameters (VDss, CNS and BBB): all compounds are poor distributed in the blood or in the bloodstream. A good VDss range was 0.5 to 3 log L/Kg. The drug candidate should not affect the central nervous system (CNS) and BBB (Blood-Brain Barrier). The drug concentration should be focused on the disease target [54-55]. BBB and CNS > 2.0 indicated strong absorption, whereas 0.1 - 2.0 indicated moderate absorption and < 0.1 indicated low absorption. Analysis of the effect of compounds 1-9 on central nervous system metabolism of CYP1A2, CYP2D6, CYP2C9, and CYP2C19 showed that all compounds did not inhibit the 4 enzymes. These enzymes were CYP isoenzymes that catalysed the metabolism of drugs so they could be digested or absorbed by the body [56]. Good drugs did not inhibit the activity of these enzymes. Compounds 1-9 exhibited substantial total clearance values, indicating how easily these compounds, particularly thymoquinone, can be secreted and their overall benefit to the body. Acute oral

toxicity analysis with the LD_{50} parameter in compounds 1-9 showed the possibility of being harmful if ingested. This parameter was used to measure how toxic or non-toxic the oral drug is when tested on rats. LD_{50} values in the range of 50 mg/kg ≤ LD_{50} > 5 mg/kg indicated the drug fatal if swallowed, toxic in the range of 300 mg/kg ≤ LD_{50} > 50 mg/kg, oral drugs could be harmful if swallowed in the range of 2000 - 5000 mg/Kg, and non-toxic in the range of LD_{50} > 5000 mg/kg [56].

The potential of a compound as an oral drug candidate can also be assessed through its physicochemical properties, particularly its compliance with Lipinski's Rule of 5 (RO5) [57]. RO5 rules must have a specific gravity of less than 500 Daltons, the number of H bond acceptors was less than 10 bonds, H bond donors were less than 5, lipophilicity was less than 5 bonds and molar refractivity was 40 - 130. A compound was allowed to be oral drug-like if there had only a maximum one deviation from the RO5 rule. RO5 analysis of compounds 1-9 was contained in **Table 7**. The compound that complied with RO5 parameters was only compound 9. Compounds 1 - 8 do not qualify as oral drugs, as they have a Violation score of 4. However, they have the potential to be used as mouthwash as an alternative to chlorhexidine [58].

Table 6 ADMET analysis results of compounds 1-9.

Properties	Parameters		1	2	3	4	5	6	7	8	9
Absorption	Intestinal Absorption (% Absorbed)		0	0	0	0	19.964	0	0	10.885	100
	Water Solubility (log mol/L)		−2.886	−2.78	−2.859	−2.892	−2.795	−2.891	−2.892	−2.884	−3.006
Distribution	BBB Permeability (log BB)		−2.567	−2.339	−2.038	−2.631	−1.542	−2.292	−2.441	−1.695	−0.152
	CNS Permeability (log PS)		−5.931	−5.048	−4.792	−5.935	−4.257	−5.05	−5.379	−3.829	−1.084
	Volume Distribution (VDss) (log L/Kg)		−0.161	−0.282	−0.217	−0.002	−0.261	−0.093	−0.06	−0.387	−1.182
Metabolism	Inhibitor of	CYP1A2	No	No	No	No	No	No	No	No	No
		CYP2D6	No	No	No	No	No	No	No	No	No
		CYP2C9	No	No	No	No	No	No	No	No	No
		CYP2C19	No	No	No	No	No	No	No	No	No
		CYP3A4	No	No	No	No	No	No	No	No	No
Excretion	Total Clearance log mL/Min/Kg		−0.023	−0.016	−0.057	−0.055	0.008	−0.091	−0.016	−0.1	−0.081
Acute Oral Toxicity	Lethal Dose 50 %mg/Kg		2.482	2.483	2.488	2.508	2.588	2.482	2.484	2.497	2.861

Table 7 Drug-Likeness Analysis of Lipinski's Rule of 5 (RO5) compounds 1-9.

Rule	Parameter	1	2	3	4	5	6	7	8	9
Lipinski's Rule of 5	Molecular mass (Less than 500 Dalton) (g/mol)	1234	1058	1058	1366	927	1189	1205	881	456
	Hydrogen bond acceptors (Less than 10)	25	21	20	29	17	24	25	15	3
	Hydrogen bond donor (Less than 5)	14	12	12	17	10	14	15	9	2
	Molar Refractivity (40 - 130)	294.68	258.65	257.56	321.17	232.23	288.78	289.95	225.59	136.65
	LogP (Less than 5)	−1.13	−0.37	−0.1	−3.42	1.17	−1.24	−2.27	2.65	7.23
	Violation	4	4	4	4	4	4	4	4	2
	Drug-likeness	No	No	No	No	No	No	No	No	Yes

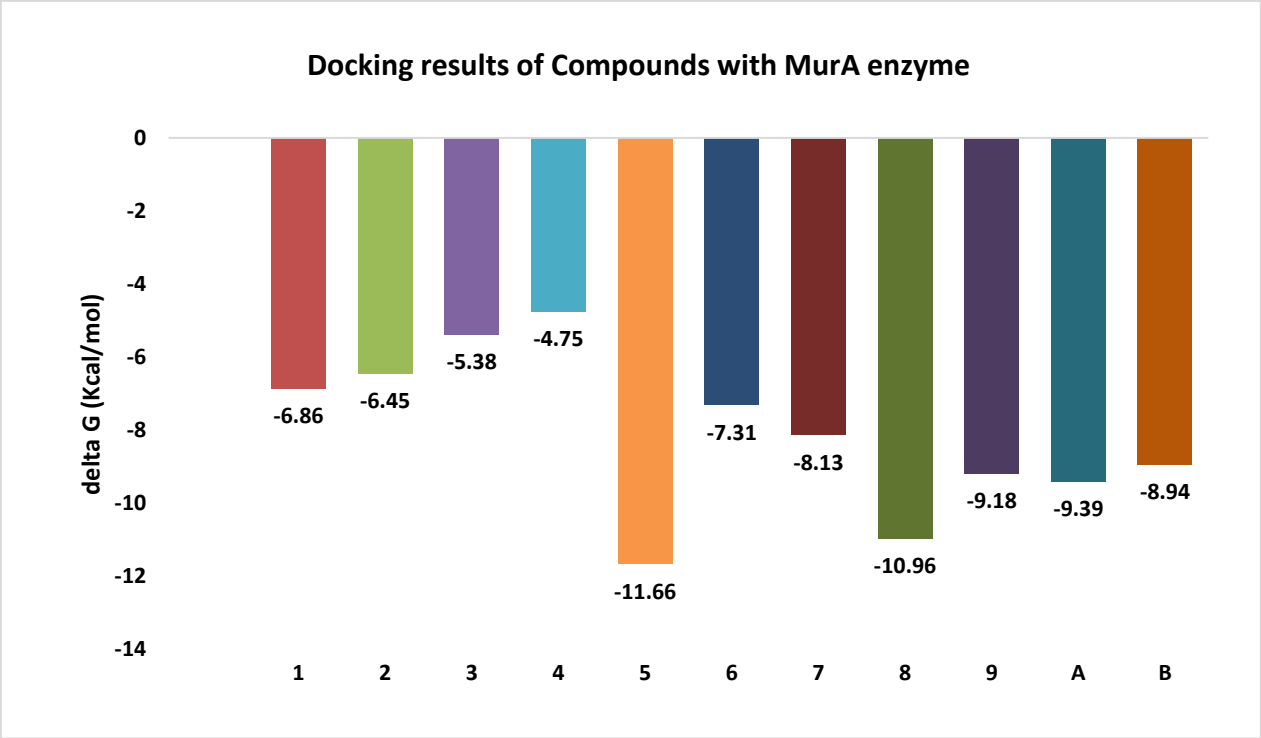

Figure 6 Graph of binding affinity (ΔG) values between compounds (1-9), apigenin (A), chlorhexidine (B) with MurA enzyme.

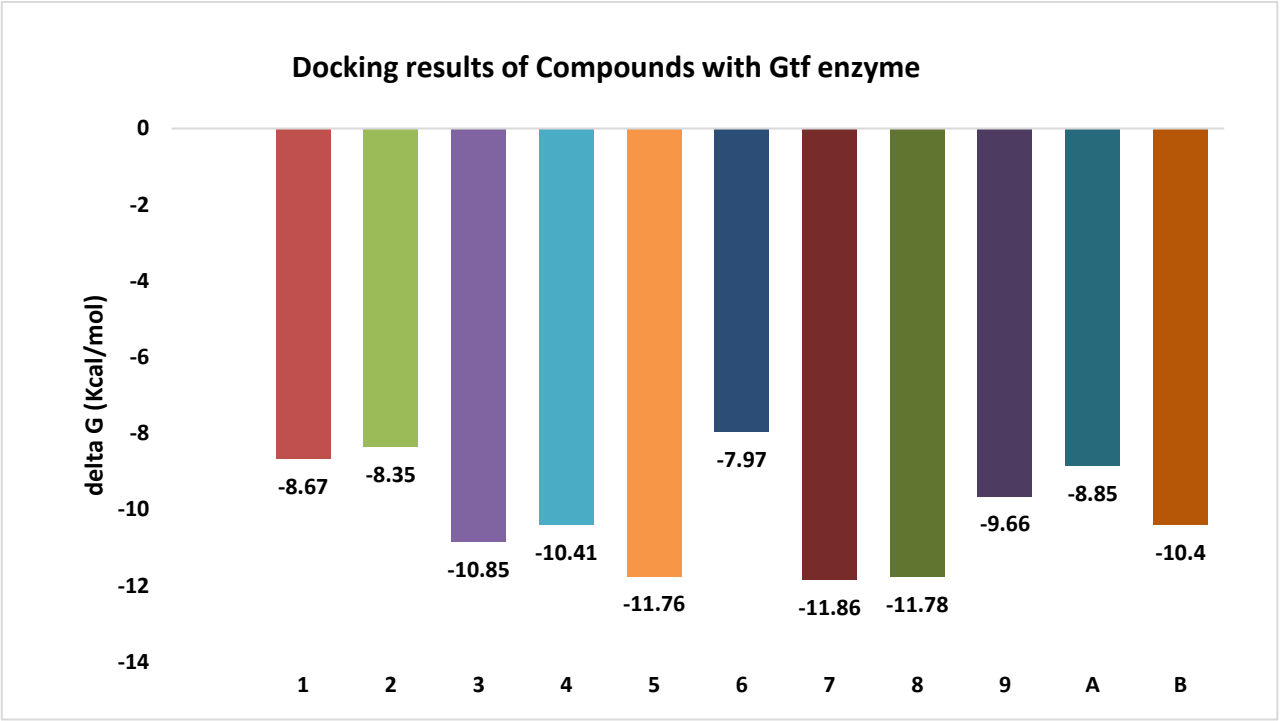

Figure 7 Graph of binding affinity (ΔG) values between compounds (1-9), apigenin (A), chlorhexidine (B) with Gtf enzyme.

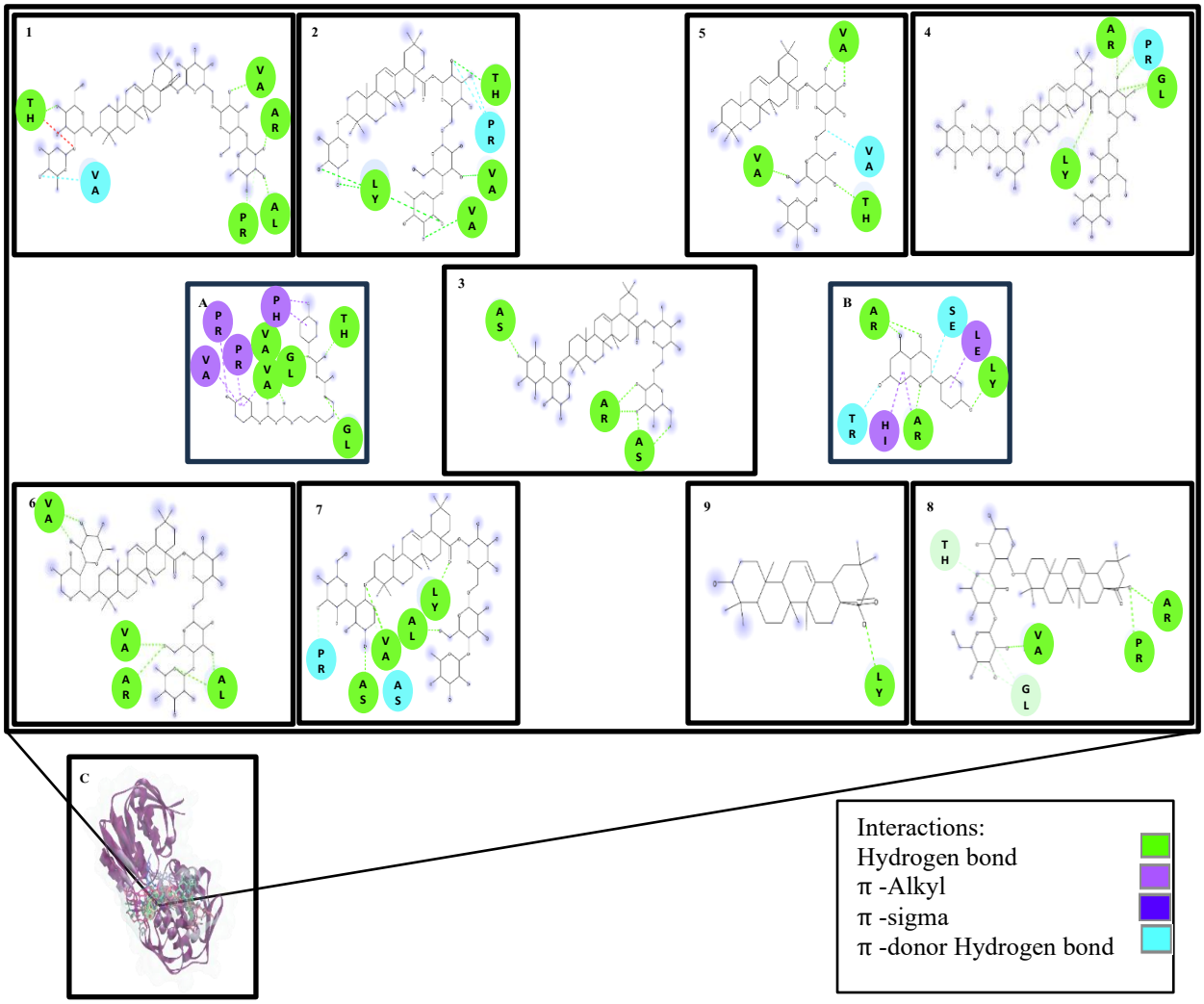

Figure 8 2D visualization of docking results of Anhuienoside E (1), Anhuienoside D (2), Anhuienoside C (3), Anhuienoside F (4), Cussonoside B (5), Flaccidoside II (6), Flaccidoside III (7), their derivatives (9), Oleanolic acid (9), Chlorhexidine (A), Apigenin (B) docked with MurA and 3D visualization (C).

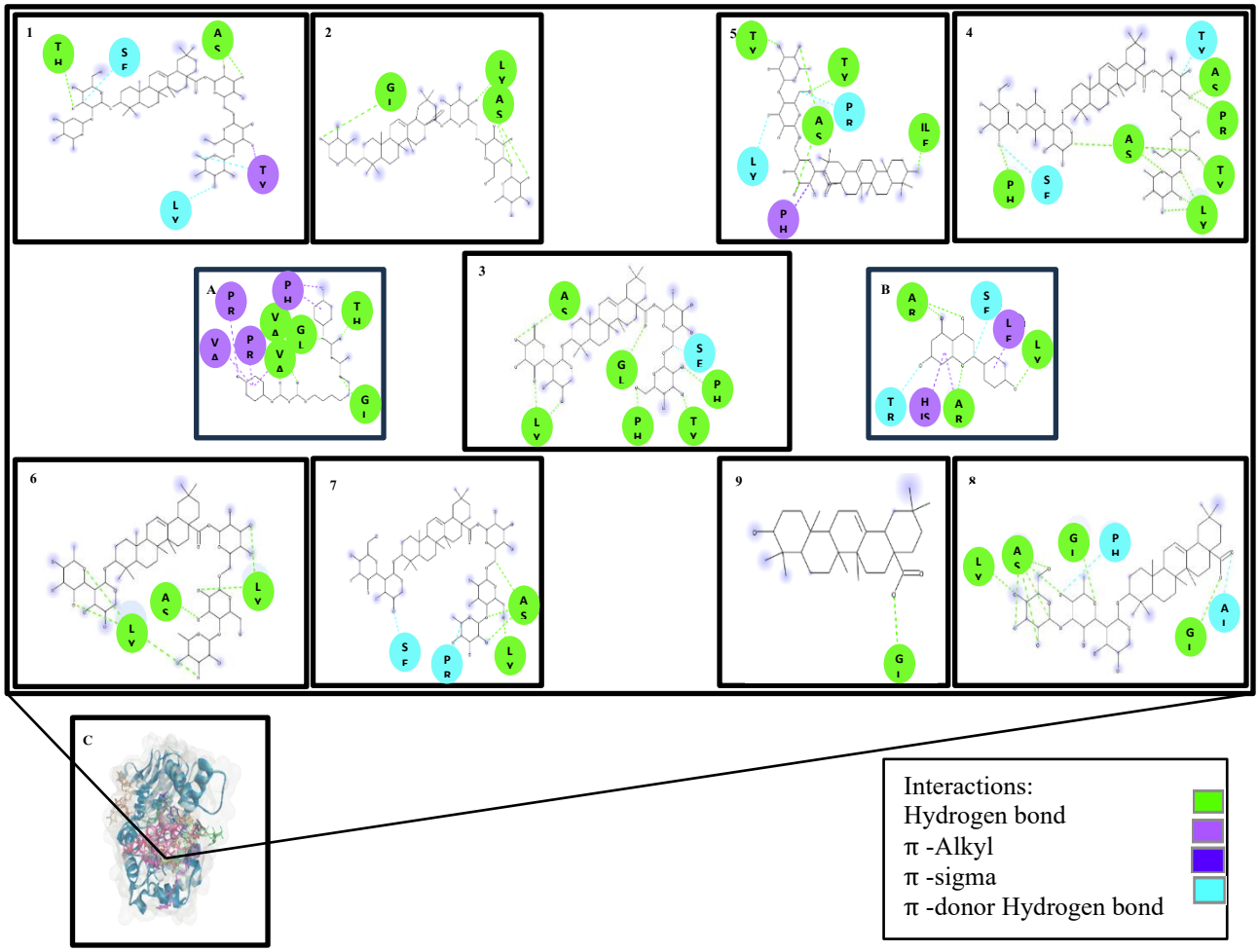

Figure 9 2D visualization of docking results of Anhuienoside E (1), Anhuienoside D (2), Anhuienoside C (3), Anhuienoside F (4), Cussonoside B (5), Flaccidoside II (6), Flaccidoside III (7), their derivatives (8), Oleanolic acid (9), Chlorhexidine (A), Apigenin (B) docked with Gtf and 3D visualization (C).

Conclusions

The pure compound Anhuienoside E (1) was successfully isolated from the methanol extract of *N. sativa* seeds and demonstrated moderate antibacterial activity against *S. mutans*, *S. sanguinis*, and *E. faecalis*. *In silico* molecular docking analysis indicated that derivatization of Anhuienoside E (1) is necessary to improve its antibacterial potency by targeting the inhibition of MurA and Gtf enzymes. ADMET and drug-likeness analyses revealed that Anhuienoside E (1) is not suitable for oral administration. However, it shows potential as a mouthwash agent and could serve as a promising alternative to chlorhexidine, which has shown increasing resistance in the treatment of dental caries. In the present study, derivatization of Anhuienoside E (1) was not performed. Further research is required to enhance its antibacterial efficacy, particularly through sugar moiety modifications aimed at MurA and Gtf enzyme inhibition.

Acknowledgements

The authors are grateful to Academic Leadership Grant (ALG) Prof. Dikdik Kurnia, M.Sc., Ph.D. Universitas Padjadjaran Indonesia for all research facilities

Declaration of Generative AI in Scientific Writing

No generative AI or AI-assisted technologies were used in the writing of this manuscript.

References

[1] R Amalia, F Chairunisa, MF Alfian and A Supartinah. Indonesia: Epidemiological profiles of early childhood caries. *Frontiers in Public Health* 2019; **7**, 210.

[2] JA Lemos, SR Palmer, L Zeng, ZT Wen, JK Kajfasz, IA Freires, J Abranches and LJ Brady. The Biology of Streptococcus mutans. *Microbiology Spectrum* 2019; **7(1)**, 1-18.

[3] S Javed, M Zakirulla, RU Baig, SM Asif and AB Meer. Development of artificial neural network model for prediction of post-streptococcus mutans in dental caries. *Computer Methods and Programs in Biomedicine* 2020; **186**, 105198.

[4] B Zhu, LC Macleod, T Kitten and P Xu. Streptococcus sanguinis biofilm formation & interaction with oral pathogens. *Future Microbiology* 2018; **13(8)**, 915-932.

[5] L Xin, Z Hu, R Han, X Xu, C Wang, D Li, Y Guo and F Hu. Asp50Glu mutation in MurA results in fosfomycin resistance in Enterococcus faecium. *Journal of Global Antimicrobial Resistance* 2022; **30**, 50-55.

[6] S Huang, M Wu, Y Li, J Du, S Chen, S Jiang, X Huang and L Zhan. The dlt operon contributes to the resistance to chlorhexidine in streptococcus mutans. *International Journal of Antimicrobial Agents* 2022; **59(3)**, 106540.

[7] Y Lin, J Chen, X Zhou and Y Li. Inhibition of Streptococcus mutans biofilm formation by strategies targeting the metabolism of exopolysaccharides. *Critical Reviews in Microbiology* 2021; **47(5)**, 667-677.

[8] MM Miyachiro, D Granato, DM Trindade, C Ebel, AFP Leme and A Dessen. Complex formation between mur enzymes from streptococcus pneumoniae. *Biochemistry* 2019; **58(30)**, 3314-3324.

[9] LD Garbinski, BP Rosen and M Yoshinaga. Organoarsenicals inhibit bacterial peptidoglycan biosynthesis by targeting the essential enzyme MurA. *Chemosphere* 2020; **254**, 126911.

[10] E Sutrisna, S Wahyuni and A Fitriani. Antibacterial effect of nigella sativa L. seed from Indonesia. *Pharmacognosy Journal* 2022; **14(6)**, 1029-1032.

[11] M Ikhsan, N Hiedayati, K Maeyama and F Nurwidya. Nigella sativa as an anti-inflammatory agent in asthma. *BMC Research Notes* 2018; **11**, 744.

[12] D Kurnia, R Padilah, E Apriyanti and HDA Dharsono. Phytochemical analysis and anti-biofilm potential that cause dental caries from black cumin seeds (nigella sativa linn.). *Drug Design, Development and Therapy* 2024; **18**, 1917-1932.

[13] A Shah, S Akhtar, F Mahmood, S Urooj, AB Siddique, MI Irfan, M Naeem-Ul-Hassan, M Sher, A Alhoshani, A Rauf, HMA Amin and A Abbas. Fagonia arabica extract-stabilized gold nanoparticles as a highly selective colorimetric nanoprobe for Cd2+ detection and as a potential photocatalytic and antibacterial agent. *Surfaces and Interfaces* 2024; **51**, 104556.

[14] S Ullah, R Khalid, MF Rehman, MI Irfan, A Abbas, A Alhoshani, F Anwar and HMA Amin. Biosynthesis of phyto-functionalized silver nanoparticles using olive fruit extract and evaluation of their antibacterial and antioxidant properties. *Frontiers in Chemistry* 2023; **11**, 1202252.

[15] A Jabbar, A Abbas, N Assad, M Naeem-ul-Hassan, HA Alhazmi, A Najmi, K Zoghebi, MA Bratty, A Hanbashi and HMA Amin. A highly selective Hg^{2+} colorimetric sensor and antimicrobial agent based on green synthesized silver nanoparticles using *Equisetum diffusum* extract. *RSC Advances* 2023; **13(41)**, 28666-28675.

[16] AB Siddique, MA Shaheen, A Abbas, Y Zaman, MA Bratty, A Najmi, A Hanbashi, M Mustaqeem, HA Alhazmi, Z ur Rehman, K Zoghebi and HMA Amin. Thermodynamic and kinetic insights into azo dyes photocatalytic degradation on biogenically synthesized ZnO nanoparticles and their antibacterial potential. *Heliyon* 2024; **10(23)**, e40679.

[17] AF Majdalawieh, SM Yousef and IA Abu-Yousef. Thymoquinone, a major constituent in Nigella sativa seeds, is a potential preventative and treatment option for atherosclerosis. *European Journal of Pharmacology* 2021; **909**, 174420.

[18] MF Mahomoodally, MZ Aumeeruddy, LJ Legoabe, D Montesano and G Zengin. Nigella sativa L. and its active compound thymoquinone in the clinical management of diabetes: A systematic review. *International Journal of Molecular Sciences* 2022; **23(20)**, 12111.

[19] P Gnanasekaran, A Roy, NS Natesh, V Raman, P Ganapathy and MK Arumugam. Removal of microbial pathogens and anticancer activity of synthesized nano-thymoquinone from Nigella sativa seeds. *Environmental Technology & Innovation* 2021; **24**, 102068.

[20] W Huang. Open tubular ion chromatography: A state-of-the-Art review. *Analytica Chimica Acta* 2021; **1143**, 210-224.

[21] S Segan, D Opsenica and D Milojkovic-Opsenica. Thin-layer chromatography in medicinal chemistry. *Journal of Liquid Chromatography and Related Technologies* 2019; **42(9-10)**, 238-248.

[22] IA Evangelina, Y Herdiyati, A Laviana, R Rikmasari, C Zubaedah, Anisah and D Kurnia. Bio-mechanism inhibitory prediction of β-sitosterol from kemangi (ocimum basilicum L.) as an inhibitor of murA enzyme of oral bacteria: *In vitro* and *in silico* Study. *Advances and Applications in Bioinformatics and Chemistry* 2021; **14**, 103-115.

[23] JR Hanson. A hundred years in the elucidation of the structures of natural products. *Science Progress* 2017; **100(1)**, 63-79.

[24] P Parvekar, J Palaskar, S Metgud, R Maria and S Dutta. The minimum inhibitory concentration (MIC) and minimum bactericidal concentration (MBC) of silver nanoparticles against Staphylococcus aureus. *Biomaterial Investigations in Dentistry* 2020; **7(1)**, 105-109.

[25] N Schormann, M Patel, L Thannickal, S Purushotham, R Wu, JL Mieher, H Wu and C Deivanayagam. The catalytic domains of streptococcus mutans glucosyltransferases: A structural analysis. *Acta Crystallographica Section F: Structural Biology Communications* 2023; **79**, 119-127.

[26] D Kurnia, GS Hutabarat, D Windaryanti, T Herlina, Y Herdiyati and MH Satari. Potential allylpyrocatechol derivatives as antibacterial agent against oral pathogen of S. Sanguinis ATCC 10,556 and as inhibitor of MurA Enzymes: *In vitro* and *in silico* study. *Drug Design, Development and Therapy* 2020; **14**, 2977-2985.

[27] OV Sobolev, PV Afonine, NW Moriarty, ML Hekkelman, RP Joosten, A Perrakis and PD Adams. A global ramachandran score identifies protein structures with unlikely stereochemistry. *Structure* 2020; **28(11)**, 1249-1258.

[28] W Tian, C Chen, X Lei, J Zhao and J Liang. CASTp 3.0: Computed atlas of surface topography of proteins. *Nucleic Acids Research* 2018; **46(W1)**, W363-W367.

[29] MS Valdes-Tresanco, ME Valdes-Tresanco, PA Valiente and E Moreno. AMDock: A versatile graphical tool for assisting molecular docking with autodock vina and autodock4. *Biology Direct* 2020; **15**, 12.

[30] LLG Ferreira and AD Andricopulo. ADMET modeling approaches in drug discovery. *Drug Discovery Today* 2019; **24(5)**, 1157-1165.

[31] A Daina, O Michielin and V Zoete. SwissADME: A free web tool to evaluate pharmacokinetics, drug-likeness and medicinal chemistry friendliness of small molecules. *Scientific Reports* 2017; **7**, 42717.

[32] C Jia, J Li, G Hao and G Yang. A drug-likeness toolbox facilitates ADMET study in drug discovery. *Drug Discovery Today* 2020; **25(1)**, 248-258.

[33] Y Bibi, S Nisa, FM Chaudhary and M Zia. Antibacterial activity of some selected medicinal plants of Pakistan. *BMC Complementary and Alternative Medicine* 2011; **11**, 52.

[34] MD Awouafack, LJ McGaw, S Gottfried, R Mbouangouere, P Tane, M Spiteller and JN Eloff. Antimicrobial activity and cytotoxicity of the ethanol extract, fractions and eight compounds isolated from Eriosema robustum (Fabaceae). *BMC Complementary and Alternative Medicine* 2013; **13**, 289.

[35] T Scrob, A Hosu and C Cimpoiu. Trends in analysis of vegetables by high performance TLC. *Journal of Liquid Chromatography and Related Technologies* 2019; **42(9-10)**, 249-257.

[36] A Pyka. Detection progress of selected drugs in TLC. *BioMed Research International* 2014; **2014(1)**, 732078.

[37] M Asemani and AR Rabbani. Detailed FTIR spectroscopy characterization of crude oil extracted asphaltenes: Curve resolve of overlapping bands. *Journal of Petroleum Science and Engineering* 2020; **185**, 106618.

[38] Y Huang, X Li, X Peng, AT Adegoke, J Chen, H Su, G Hu, G Wei and M Qiu. NMR-based structural classification, identification, and quantification of triterpenoids from edible mushroom ganoderma resinaceum. *Journal of Agricultural and Food Chemistry* 2020; **68(9)**, 2816-2825.

[39] Q Shi, J Yan, B Jiang, X Chi, J Wang, X Liang and X Ai. A general strategy for the structural determination of carbohydrates by multi-dimensional NMR spectroscopies. *Carbohydrate Polymers* 2021; **267**, 118218.

[40] S Qiu, N Van Hung, LT Xuan, J Gu, E Lobkovsky, TC Khanh, DD Soejarto, J Clardy, JM Pezzuto, Y Dong, MV Tri, LM Huong and HHS Fong. A pregnane steroid from Aglaia lawii and structure confirmation of cabraleadiol monoacetate by X-ray crystallography. 2001; **56(7)**, 775-780.

[41] A Furevi, A Ruda, TA D'Ortoli, H Mobarak, J Stahle, C Hamark, C Fontana, O Engstrom, P Apostolica and G Widmalm. Complete 1H and 13C NMR chemical shift assignments of mono-to tetrasaccharides as basis for NMR chemical shift predictions of oligo- and polysaccharides using the computer program CASPER. *Carbohydrate Research* 2022; **513**, 108528.

[42] S Belarbi, M Vivier, W Zaghouani, AD Sloovere, V Agasse-Peulon and P Cardinael. Comparison of new approach of GC-HRMS (Q-Orbitrap) to GC–MS/MS (triple-quadrupole) in analyzing the pesticide residues and contaminants in complex food matrices. *Food Chemistry* 2021; **359**, 129932.

[43] WC Ye, QW Zhang, SX Zhao and CT Che. Four new oleanane saponins from anemone anhuiensis. *Chemical and Pharmaceutical Bulletin* 2001; **49(5)**, 632-634.

[44] SB Tankeo, F Damen, MD Awouafack, J Mpetga, P Tane, JN Eloff and V Kuete. Antibacterial activities of the methanol extracts, fractions and compounds from Fagara tessmannii. *Journal of Ethnopharmacology* 2015; **169**, 275-279.

[45] PY Chung. Novel targets of pentacyclic triterpenoids in staphylococcus aureus: A systematic review. *Phytomedicine* 2020; **73**, 152933.

[46] M Zhao, N Zhang, T Gao, J Jin, T Jing, J Wang, Y Wu, X Wan, W Schwab and C Song. Sesquiterpene glucosylation mediated by glucosyltransferase UGT91Q2 is involved in the modulation of cold stress tolerance in tea plants. *New Phytologist* 2020; **226(2)**, 362-372.

[47] SW Park, BH Lee, SH Song, and MK Kim. Revisiting the Ramachandran plot based on statistical analysis of static and dynamic characteristics of protein structures. *Journal of Structural Biology* 2023; **215**, 107939.

[48] P Chakrabarti and D Pal. The interrelationships of side-chain and main-chain conformations in proteins 2001; **76(1-2)**, 1-102.

[49] GD Rose. Ramachandran maps for side chains in globular proteins. *Proteins: Structure, Function and Bioinformatics* 2019; **87(5)**, 357-364.

[50] KD Wild, F Porrecaf, HI Yamamurat and RB Raffa. Differentiation of receptor subtypes by thermodynamic analysis: Application to opioid 6 receptors 1994; **91(25)**, 12018-12021.

[51] F Azimi, H Azizian, M Najafi, F Hassanzadeh, H Sadeghi-aliabadi, JB Ghasemi, M Ali Faramarzi, S Mojtabavi, B Larijani, L Saghaei and M Mahdavi. Design and synthesis of novel quinazolinone-pyrazole derivatives as potential α-glucosidase inhibitors: Structure-activity relationship, molecular modeling and kinetic study. *Bioorganic Chemistry* 2021; **114**, 105127.

[52] J Song, X Jin, XC Wang and P Jin. Preferential binding properties of carboxyl and hydroxyl groups with aluminium salts for humic acid removal. *Chemosphere* 2019; **234**, 478-487.

[53] F Ntie-Kang. An *in silico* evaluation of the ADMET profile of the StreptomeDB database. *SpringerPlus* 2013; **2**, 353.

[54] TJ Hou and XJ Xu. ADME evaluation in drug discovery. 3. modeling blood-brain barrier partitioning using simple molecular descriptors. *Journal of Chemical Information and Computer Sciences* 2003; **43(6)**, 2137-2152.

[55] L Zhu, J Zhao, Y Zhang, W Zhou, L Yin, Y Wang, Y Fan, Y Chen and H Liu. ADME properties

evaluation in drug discovery: *In silico* prediction of blood–brain partitioning. *Molecular Diversity* 2018; **22**, 979-990.

[56] T Siswina, MM Rustama, D Sumiarsa, E Apriyanti, H Dohi and D Kurnia. Antifungal constituents of piper crocatum and their activities as ergosterol biosynthesis inhibitors discovered via *in silico* study using ADMET and drug-likeness analysis. *Molecules* 2023; **28(23)**, 7705.

[57] CA Lipinski. Lead- and drug-like compounds: The rule-of-five revolution. *Drug Discovery Today: Technologies* 2004; **1(4)**, 337-341.

[58] MP Pollastri. Overview on the rule of five. *Current Protocols in Pharmacology* 2010; **49(1)**, 9.12.1-9.12.8.